HEALTH AND MEDICINE



# Microneedle-assisted genome editing: A transdermal strategy of targeting *NLRP3* by CRISPR-Cas9 for synergistic therapy of inflammatory skin disorders

**Tao Wan*, Qi Pan*, Yuan Ping†**

**We report a dissolvable microneedle (MN) patch that can mediate transdermal codelivery of CRISPR-Cas9–based genome-editing agents and glucocorticoids for the effective treatment of inflammatory skin disorders (ISDs). The MN is loaded with polymer-encapsulated Cas9 ribonucleoprotein (RNP) targeting *NLRP3* and dexamethasone (Dex)–containing polymeric nanoparticles. Upon insertion into the skin, the MN can be dissolved quickly to release two types of nanoformulations, which are subsequently internalized by keratinocytes and surrounding immune cells to exert their therapeutic effects in the inflammatory subcutaneous layers. Thus, the MN-enabled transdermal codelivery of Cas9 RNP nanocomplexes and Dex nanoparticles result in the disruption of subcutaneous intracellular NLRP3 inflammasomes, which is demonstrated to be critical to alleviate skin inflammations and contributes to glucocorticoid therapy in mouse models of ISDs, including psoriasis and atopic dermatitis. Our study offers innovative insights into the rational design of transdermal delivery systems and defines an effective therapeutic option for the treatment of ISDs.**

## INTRODUCTION

Inflammatory skin disorders (ISDs) represent one of the most persistent diseases that are generally characterized by the activation of the innate and adaptive immune responses through the production of proinflammatory cytokines (*1*). ISDs such as psoriasis and atopic dermatitis (AD) are becoming the major issues threatening public health with increasing prevalence. These disorders are generally considered as a result of the inflammatory responses of the epithelial barrier of the skin against allergens and pathogens (*1*). For example, the pathogenesis of psoriasis is typically indicated by the abnormal activation of dendritic cells and T cell–mediated autoimmune responses with complex cellular networks (*2*, *3*). As another representative inflammatory dermatopathy, the pathogenesis of AD is generally characterized by dominant T helper 2 cell ($T_H2$)–mediated abnormal inflammatory responses and elevated levels of both eosinophils and serum immunoglobulin E (IgE) (*4*, *5*). Currently, patients who suffered from these disorders are limited to a few approved therapeutic options. Although topical glucocorticoid and immunosuppressive agents remain to be the first-line treatment modality, most patients often show poor responses to topical or systemic glucocorticoid therapy as a result of glucocorticoid resistance, especially for the long-term treatment (*3*, *5*, *6*). This suggests that alternative therapeutic options are essential to sensitize the glucocorticoid resistance or to improve the glucocorticoid therapy.

Inflammasomes are supramolecular complexes of inflammatory proteins, which are responsible for the activation of inflammatory responses and the identification of pathogens in the development of inherent immunity (*7*). Among various subtypes of inflammasomes, nod-like receptor family, pyrin domain–containing 3 (NLRP3) has been associated with a variety of inflammatory and autoimmune skin conditions, including psoriasis and AD, and its activation is relevant to a number of allergic stimuli in the inflammatory processes (*8*–*10*). Accumulating evidence indicates that the overexpression of CASP-1 (encoding caspase-1) and the up-regulation of its activator, NLRP3 inflammasome, in inflammatory diseases can cause glucocorticoid resistance (*11*). The NLRP3–CASP-1 inflammasome modulates cellular levels of the functional glucocorticoid receptor in its transactivation domain and diminishes glucocorticoid transcriptional effects to increase glucocorticoid resistance in immune-related cells (*11*). However, the overexpression of CASP-1 without its activation via NLRP3 inflammasome did not alter the glucocorticoid sensitivity of immune-related cells, suggesting the strong association between *NLRP3* activation and glucocorticoid resistance (*11*, *12*). Given the critical role of NLRP3 inflammasome in the pathogenesis of ISDs, recent efforts have been dedicated to targeting NLRP3 inflammasomes to alleviate inflammatory responses (*13*). To this end, small molecular inhibitors have been actively investigated for their potential to target NLRP3 inflammasomes to treat ISDs in recent years. For example, cycloastragenol, a small molecule isolated from *Astragalus membranaceus*, has shown good ability to ameliorate the typical clinical symptoms of psoriasis in the mouse model by inhibiting NLRP3 inflammasome–mediated pyroptosis in macrophages (*14*). As demonstrated in another study, the oral administration of small molecule CP-456,773, a well-studied specific NLRP3 inhibitor, could reduce skin inflammation by preventing inflammasome activation (*15*). To improve therapeutic efficacy and safety, it is imperative to design inhibitors that can target NLRP3 in a direct and specific manner. Nevertheless, most well-studied small-molecule inhibitors, such as CY-09, usually indirectly inhibit the function of NLRP3 inflammasome by regulating upstream events associated with its activation (*16*). Furthermore, despite promising antagonistic effects against NLRP3, these small molecules only showed moderate effects because NLRP3 inflammasomes are primarily located at the epidermal and dermal layers of the human skin, whereas the oral administration of these inhibitors only leads to the limited access to the subcutaneous layer. For effective delivery, it is essential to consider the skin barriers that prevent the entry of the inhibitors at different levels. Thus, the efficient transdermal delivery of a highly specific, powerful, and direct NLRP3 inhibitor seems to be an ideal promising strategy to combat ISDs.

College of Pharmaceutical Sciences, Zhejiang University, Hangzhou 310058, China.
*These authors contributed equally to this work.
†Corresponding author. Email: pingy@zju.edu.cn

We here report a microneedle (MN) patch for the transdermal codelivery of the RNA-guided clustered regularly interspaced short palindromic repeat–associated nuclease protein 9 (CRISPR-Cas9)–based genome-editing agents and glucocorticoids for the effective treatment of ISDs. As shown in Fig. 1, the MN patch is designed as follows: (i) polymer/Cas9 ribonucleoprotein (RNP) nanocomplexes for the intracellular delivery of Cas9 targeting NLRP3 inflammasome, (ii) dexamethasone (Dex)–loaded polymeric nanoparticles for the improved glucocorticoid therapy, and (iii) a dissolvable MN patch embedded with both Cas9 nanocomplexes and Dex nanoparticles for the transdermal codelivery of two nanoformulations. As a widely explored genome-editing tool, CRISPR-Cas9 has been recently harnessed as a specific inhibitor for targeting NLRP3 inflammasome to ameliorate inflammatory diseases (*17*). In principle, the direct disruption of *NLRP3* by CRISPR-Cas9–based genome editing not only inhibits the *NLRP3* activation at the DNA level but also contributes to minimizing off-target effects that many small-molecule inhibitors commonly encounter. The intracellular delivery of Cas9 RNP, enabled by the polymeric carrier that we have developed recently (*18*), ensures the efficient genome editing of *NLRP3* gene within subcutaneous keratinocytes and immune cells. In the meantime, the disruption of NLRP3 inflammasomes can further improve the sensitivity of glucocorticoid therapy. As Dex is well documented for its ability to induce the dilation of nuclear pores during its translocation process, the intracellular delivery of Dex will simultaneously contribute to the nuclear entry of genome-editing agents (*19*). Furthermore, by using hyaluronic acid (HA) and collagen tripeptide (CTP) as the matrix materials, the MN patch that we have fabricated not only has good biocompatibility but also promotes collagen synthesis, reduces transepidermal water loss (TEWL), and facilitates the tissue repair of skin lesions (*20*). Therefore, the dissolvable MN patch can greatly promote the transdermal delivery of these two nanoformulations. Collectively, the combination of genome editing of *NLRP3* and glucocorticoid therapy, which is enabled by MN-mediated transdermal delivery, is expected to be a potential, effective strategy for the treatment of ISDs.

## RESULTS

### Characterization of MN patch

The MN patch was fabricated from an aqueous solution of biocompatible HA and CTP via a micromolding approach (fig. S1). The dimension of the prepared MN array patch was 8 mm by 8 mm, with a 15-by-15 MN array. The scanning electron microscopy (SEM) images demonstrated that MN was pyramidal with a base diameter of 200 μm and a height of 600 μm (Fig. 2A), coupled with an intact and uniform morphology (fig. S2). As shown in Fig. 2B, the increase of CTP concentration affected the stiffness of MN when the content increased from 0 to 10%. The MN patch containing 10% CTP exhibited a mechanical strength of 1.5 N per needle, which is higher than that of the MN patch without CTP (0.9 N per needle). In addition, there is no substantial difference in mechanical strength between the MN patch containing 10% CTP and the MN patch containing 20% CTP. The excellent mechanical property of the fabricated MN patch ensures a sufficient stiffness for skin insertion and penetration. Despite these merits, when CTP content increased from 10 to 30%, the surface roughness of MN was obviously altered, as confirmed by SEM (Fig. 2A and fig. S3). Thus, HA and 10% CTP were used as the matrix materials. To achieve a sustained release behavior, we prepared Dex-loaded poly(lactic-*co*-glycolic acid) (PLGA)

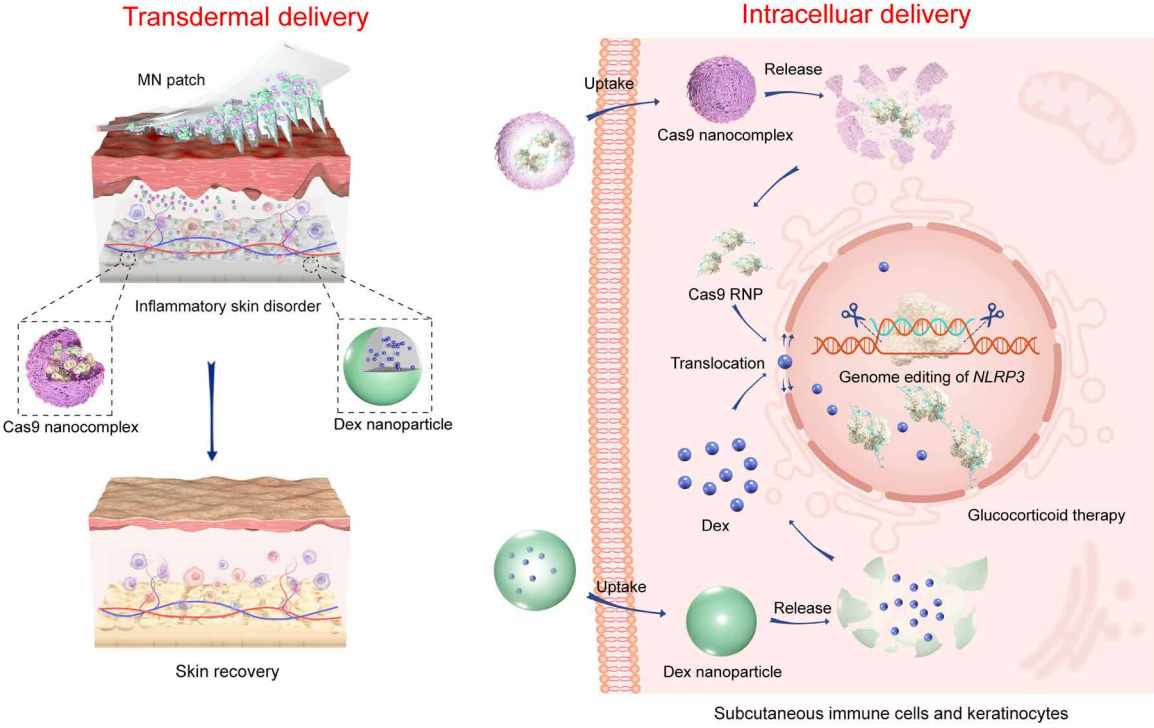


**Fig. 1. Schematic illustration of stepwise transdermal and intracellular delivery of genome-editing agents (Cas9) and glucocorticoids (Dex) for the treatment of ISDs.**

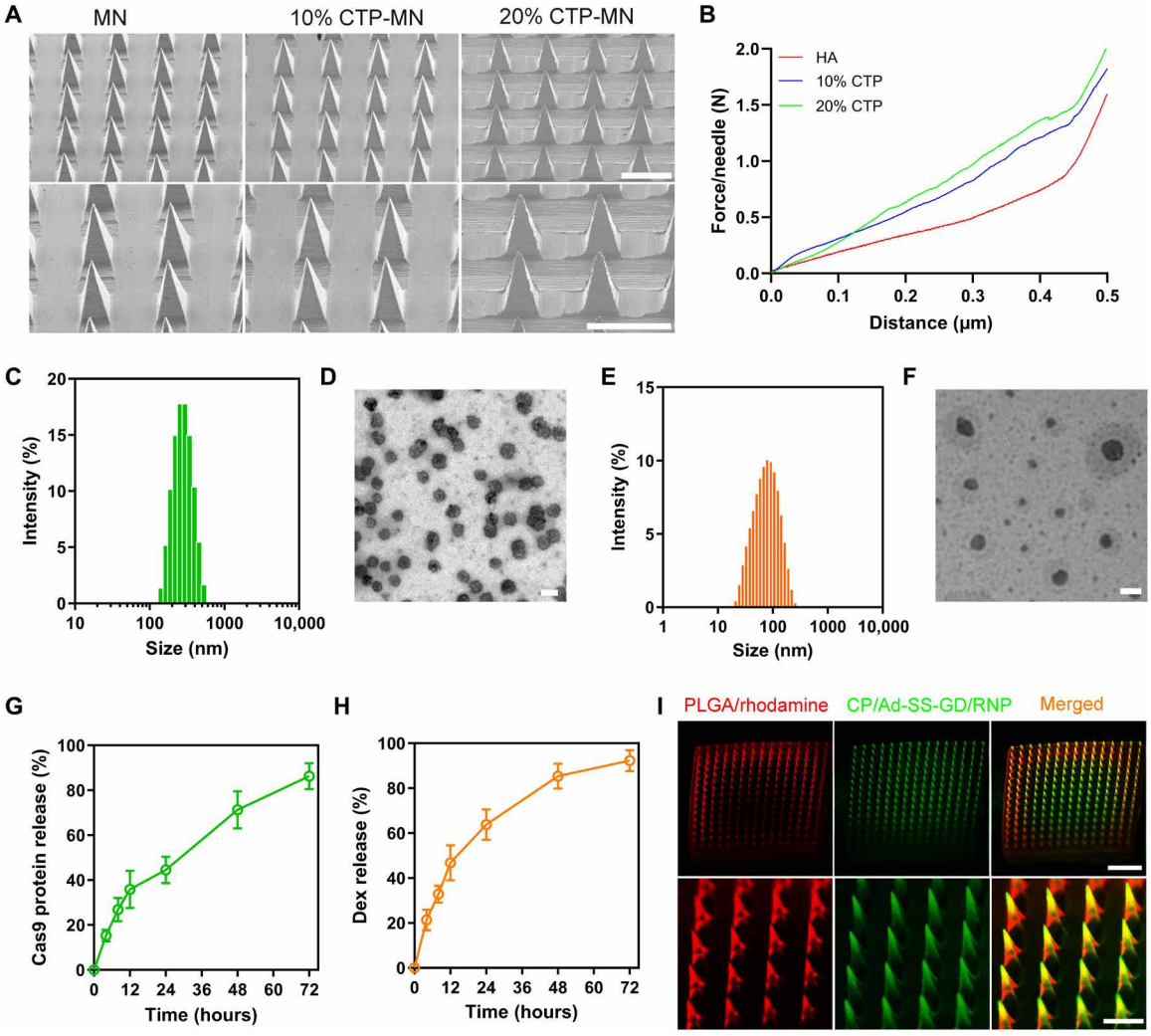


**Fig. 2. Characterization of the physical properties and drug release profiles of the dual MN system.** (**A**) SEM images of the MN patches. Scale bars, 500 μm. (**B**) Characterization of the mechanical strength of the MN patches. (**C**) DLS analysis of CP/Ad-SS-GD/Cas9 RNP nanoparticles. (**D**) TEM image of CP/Ad-SS-GD/Cas9 RNP nanoparticles. Scale bar, 200 nm. (**E**) DLS analysis of Dex-loaded PLGA nanoparticles. (**F**) TEM image of Dex-loaded PLGA nanoparticles. Scale bar, 100 nm. (**G** and **H**) In vitro collective release of Cas9 protein (G) and Dex (H) from the MN patch. Error bars represent the SE (means ± SD, $n = 6$). (**I**) Fluorescence images of MN patch containing Cas9-FITC–loaded CP/Ad-SS-GD nanoparticles and rhodamine-loaded PLGA nanoparticles. Scale bars, 2000 μm (top) and 500 μm (bottom).

nanoparticles by an emulsion/solvent evaporation method (*21*), with an average diameter of about 90 nm, as confirmed by transmission electron microscopy (TEM) and dynamic light scattering (DLS) (Fig. 2, C and D). In the previous study, we have shown that the supramolecular polymer (termed CP/Ad-SS-GD) can mediate the efficient delivery of Cas9 RNPs. In this study, CP/Ad-SS-GD/RNP was used to encapsulate Cas9 RNP targeting *NLRP3* and nanocomplexes around 200 nm that were obtained in a narrow size distribution (Fig. 2, E and F). The loading capacities of Cas9 protein and Dex were 20 and 60 μg in the MNs, respectively. Figure 2 (G and H) shows the in vitro Dex and Cas9 protein release profile from the MN. The release of Cas9 protein from the MN showed a sustained manner, which is similar to the release profile of Dex. Figure 1I exhibits the fluorescence images of a representative MN patch that contained PLGA/rhodamine nanoparticles and CP/Ad-SS-GD/Cas9 RNP–fluorescein isothiocyanate (FITC) nanoparticles. It was observed that the encapsulated nanoparticles were uniformly distributed inside the MNs. The above results suggested that the MN patch was fabricated successfully and was loaded with both Cas9 RNP nanocomplexes and Dex nanoparticles.

## Penetration ability and degradation of MN in vivo

To investigate the in vivo degradation of the MN patch, we evaluated the releases of therapeutic agents, rhodamine B from PLGA, and Cas9-FITC from CP/Ad-SS-GD, respectively. As shown in Fig. 3A, the MN patch could be successfully inserted into the skin of the mouse, with a depth of about 300 μm. Upon insertion into the mouse skin, MN could rapidly absorb the fluid from cutaneous tissues and dissolve quickly, as evidenced by the SEM image (fig. S4). In the meantime, rhodamine and Cas9-FITC were observed to distribute in the epidermal and dermal areas. The fluorescent images of the mouse skin treated by the MN patch loaded with PLGA/rhodamine B and CP/Ad-SS-GD/Cas9-FITC verified the sustained release of Dex and Cas9 protein in vivo, indicating that the MNs could act as a

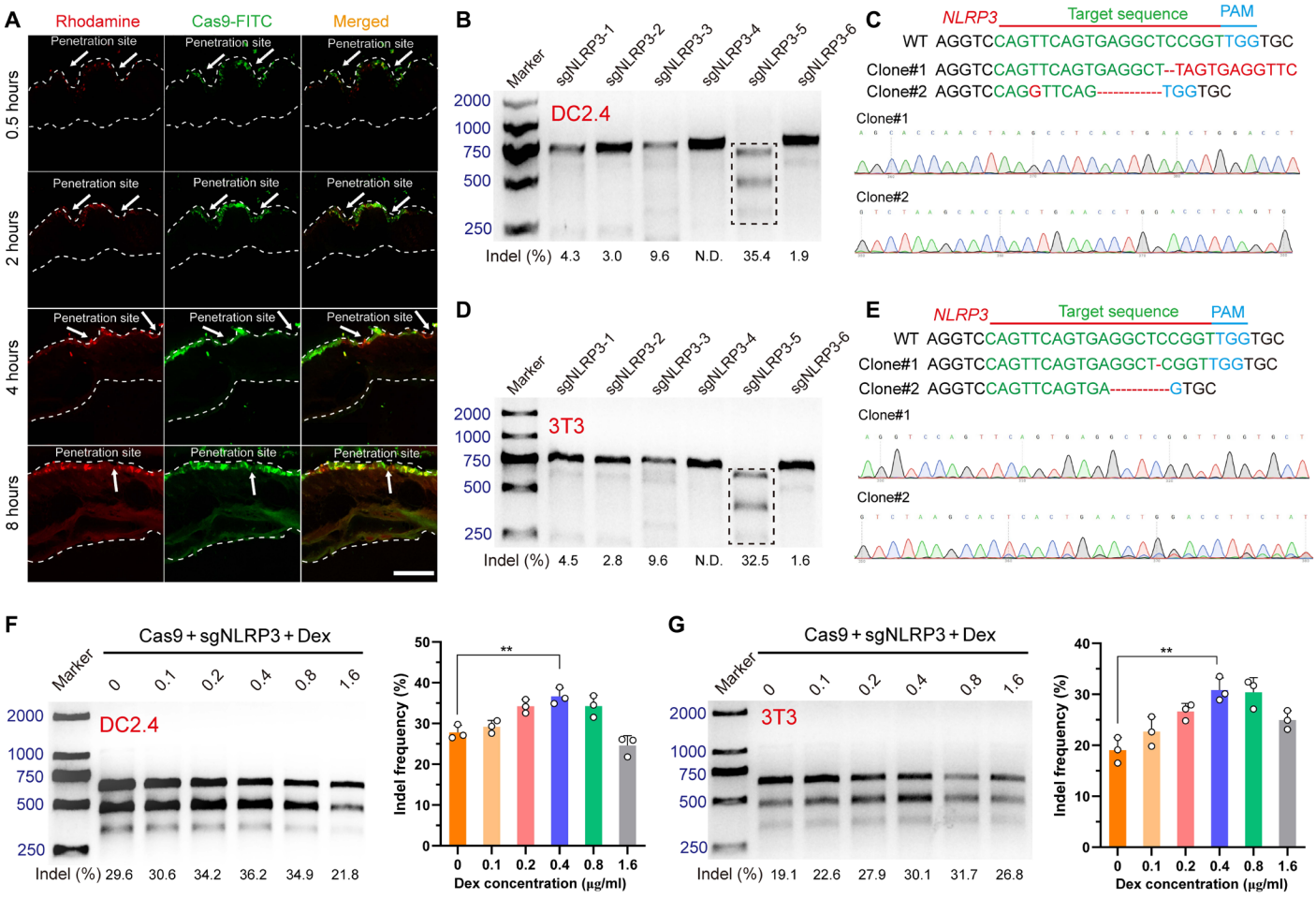


**Fig. 3. Penetration ability and degradation of MN in vivo and improved genome-editing effects of CP/Ad-SS-GD/RNP nanoparticles.** (**A**) Fluorescence images of the mouse skin recorded at different time points after insertion of the MN patch into the skin. Scale bar, 500 μm. (**B** to **E**) Screening targeting sequence of sgNLRP3 to optimize the genome-editing efficiency in DC2.4 cells (B) and 3T3 cells (D) and Sanger sequencing results of T-A cloning from DC2.4 cells (C) and 3T3 cells (E) after CMAX-mediated transfection. WT, wild type; N.D., not detectable. (**F** and **G**) T7E1 assay of indels introduced into the *NLRP3* locus in DC2.4 cells (F) and 3T3 cells (G) transfected with dual CP/Ad-SS-GD/RNP and PLGA/Dex nanoparticles. Means ± SD, $n = 3$, Student's $t$ test, $^{**}P < 0.01$.

depot inside the skin for the sustained release of therapeutics. To further investigate the in vivo biocompatibility of the MN patch, we compared the skin tissue sections 24 hours after administration with phosphate-buffered saline (PBS) and the MN patch. It was found that the skin recovered quickly after the insertion of MN, and there was no notable inflammation observed in the region where the MN was inserted, as compared with the surrounding tissue without any treatments (fig. S5). These results suggested that the MN patch system could be degraded quickly in vivo after penetration into the skin to release CP/Ad-SS-GD/RNP and PLGA/Dex nanoparticles. Furthermore, we evaluated the systemic toxicity after the MN patch–mediated therapy. To this end, the hepatotoxicity (as reflected by alanine transaminase and aspartate transaminase levels) and the nephrotoxicity (as reflected by creatinine, uric acid, and blood urea nitrogen levels) were evaluated after the indicated treatment. As shown in fig. S6, all the MN-mediated treatments were all close to the control group (without any treatment), suggesting minimal systemic toxicity. Therefore, the function index of blood biochemistry validated that the MN patch–mediated therapy merely caused any damage to the liver and the kidney, featuring its safety for future clinical translation.

## Improved genome-editing effects of CP/Ad-SS-GD/RNP

By screening different sequences of single-guide RNAs (sgRNAs) (Fig. 3B), we found that the most efficient genome editing at the *NLRP3* locus in DC2.4 cells mediated by Lipofectamine CRISPRMAX (CMAX, a commercial transfection reagent) caused a frequency of indels (insertions and deletions) up to 35.4%. As evident from Fig. 3B, after the intracellular delivery, the obvious digestion bands (cuts) were observed from the uncut bands in the *NLRP3*-5 locus. The representative sequences of indels in the *NLRP3*-5 locus of DC2.4 cells treated with CMAX/RNP are shown in Fig. 3C. Sanger sequencing confirmed the mutations at the targeted loci, including base deletion, insertion, and substitution around the protospacer adjacent motif (PAM). Similarly, genome editing targeting *NLRP3* in 3T3 cells, mediated by CMAX, caused an indel frequency up to 32.5% (Fig. 3D) and was confirmed by Sanger sequencing (Fig. 3E). On the basis of the above optimization, we further explored the genome-editing

activity mediated by CP/Ad-SS-GD in the presence of Dex-loaded PLGA nanoparticles in DC2.4 and 3T3 cells. By varying the total concentration of Dex in the cell culture, we found that the indel frequency in *NLRP3* genome locus improved from 29.6 to 36.2% after the addition of PLGA/Dex nanoparticles (at a total Dex concentration of 0.4 μg/ml) in DC2.4 cells (Fig. 3F). Similarly, the indel frequency also improved from 19.1 to 31.7% in 3T3 cells in the presence of PLGA/Dex nanoparticles (at a total Dex concentration of 0.8 μg/ml) (Fig. 3G). In addition, we also treated the cells with polymer/RNP and PLGA/Dex nanoparticles simultaneously to investigate whether there is any difference from separate treatment. The indel frequency was then analyzed through deep sequencing (figs. S7 to S10). As shown in figs. S7 and S8, two different treatments resulted in similar mutation frequencies in general. The presence of PLGA/Dex nanoparticles did not affect the cell viability at the concentration of Dex from 0.1 to 0.4 μg/ml and became slightly cytotoxic when the concentration of Dex reached 0.8 μg/ml, implying the dose-dependent cytotoxicity of PLGA/Dex nanoparticles (fig. S11). As a result, at higher Dex concentrations, the cytosolic delivery of Cas9 RNP may be affected in poorly viable cells, thereby impairing the gene-editing capacity (*22*). These results confirmed that Dex delivered by PLGA nanoparticles may potentially dilate nuclear pores to facilitate the translocation of Cas9 from the cytoplasm to the nuclei to promote genome-editing activity toward *NLRP3*.

### Treatment of AD by MN patch

To evaluate the therapeutic potential of the MN patch against skin inflammation, we first established the mouse model of AD by smearing 2,4-dinitrochlorobenzene (DNCB) on the naked dorsal skin, where MN patches were applied topically for the consecutive 5 weeks (Fig. 4A). As shown in Fig. 4B, the repeated applications of DNCB to the mouse dorsal skin induced typical lesions, such as skin dryness, severe erythema, hemorrhage, scarring, edema, excoriation, and erosion. Whereas a blank MN patch merely exhibited any therapeutic effects, an MN patch loaded with either CP/Ad-SS-GD/Cas9 or PLGA/Dex could moderately alleviate AD symptoms, which is equivalent to the therapeutic effects of commercial topical Dex cream or tacrolimus ointment. Among these various treatments, dual MN patch (RNP- and Dex-loaded MN patch) exhibited the strongest anti-inflammatory ability. Substantial alleviations in skin edema, hemorrhage, erythema, excoriation, and erosion were clearly observed in the mouse treated with dual MN patch. In addition, hair regrowth was also observed in the mouse back after the treatment by MN patches for 5 weeks. No substantial body weight loss was recorded with the mice treated by the MN patch during the therapeutic period, suggesting its safe characteristics for future clinical translation (Fig. 4C). In addition, as the major symptom of AD, pruritus is exacerbated during nocturnal sleep, which can significantly disturb the quality of life (*23*). Hindlimb scratching is associated with itch sensation in the model mouse of AD, and the alleviation of pruritus, as an indication of AD recovery, is a critical index to judge whether the treatment of AD is successful. As shown in Fig. 4D, as compared with the control group, we found that the therapy with either RNP-loaded or Dex-loaded MN patch significantly alleviated scratching behaviors in AD mice. As expected, dual MN patch exhibited the strongest inhibition against pruritus owing to the synergistic therapeutic effects of genomic disruption of *NLRP3* and glucocorticoid therapy. In addition, since the release of inflammatory cytokines, as a strong indicator of immune responses, can significantly enlarge the spleen along with weight increase in the DNCB-induced mice, the increase in weight and size of the spleen from AD mice was obviously observed. In contrast, the spleen of DNCB-induced mice treated by dual MN patch appeared to be similar in terms of weight and size as compared with the negative control group (mice without DNCB treatments) (Fig. 4, E and F). In addition, the total dermatitis scores of erythema/hemorrhage, scarring/dryness, edema, and excoriation/erosion were evaluated according to the scoring system as previously described (Fig. 4, I and J) (*24*). In agreement with the above findings, the clinical scores of dermatitis severity also significantly decreased in the dual MN patch group, suggesting the excellent ability of MN patch to treat AD. We also evaluated the reduction in TEWL value associated with skin barrier functions. As shown in Fig. 4G, the decreased level of TEWL was found when the topical treatment was carried out by blank MN patch, Dex-loaded MN patch, RNP-loaded MN patch, or dual MN patch, as compared to the negative control group. These results indicated that MN formulations containing CTP is beneficial to accelerate the repairment of the natural barrier functions of the skin. As shown in Fig. 4H, all MN treatments increased skin hydration, in comparison to the negative control group (AD mice without any treatment). Note that Dex cream and tacrolimus ointment, both of which are clinically available for the treatment of AD, could not decrease TEWL levels and increase skin hydration. Furthermore, histological analysis indicated notable skin lesions, such as epidermal hyperplasia and edema, and the accumulation of inflammatory cells were observed in the dermis/epidermis in DNCB-treated mice (Fig. 5, A and B). In contrast, the treatment with dual MN patch significantly alleviated these AD skin lesions in the dermis/epidermis in comparison to the treatment by either RNP-loaded or Dex-loaded MN patch. These findings were further supported by the reduced weight of punch biopsy specimens (fig. S12), suggesting the reduction of skin edema by dual MN patch–mediated treatment. As previous reports revealed that the infiltration of mast cells into the dermis is commonly observed in AD (*25*, *26*), we also showed that the topical application of dual MN patch could significantly reduce the infiltration of dermal mast cells through toluidine blue staining of skin tissues (Fig. 5, C and D).

Next, we evaluate the indel frequency at target genome in vivo by T7 endonuclease I (T7E1) assay. In normal mice, the topical application of MN patch resulted in the obvious genome disruption at the *NLRP3* site (14.8% indel mutation) in the epidermal and dermal tissues. Although the repeated applications of MN patch could significantly increase the genome-editing efficiency in vivo after the first treatment (fig. S13), the efficacy only slightly increased by further treatments. As it was reported previously that the preexisting immunity to Cas9 could limit gene-editing capacity in vivo (*27*, *28*), we thus measured the levels of Cas9 antibodies generated in mice after the repeated administration of dual MN patch by enzyme-linked immunosorbent assay (ELISA). As shown in fig. S14, the level of antibodies against Cas9 increased after the double treatments, becoming clearly detectable after the triple treatments. On the basis of the evidence, the repeated applications of MN patch, which is likely to cause the subsequent immune response by generating antibodies against Cas9 protein, may impair the genome-editing capability of Cas9. In AD mice, the indel frequency in the *NLRP3* locus induced by the RNP-loaded MN patch was 13.6% (Fig. 6A) and increased to 21.4% after the treatment by dual MN patch, indicating the contribution of Dex for the improved genome-editing activity in vivo. Sanger sequencing and deep sequencing confirmed the genomic

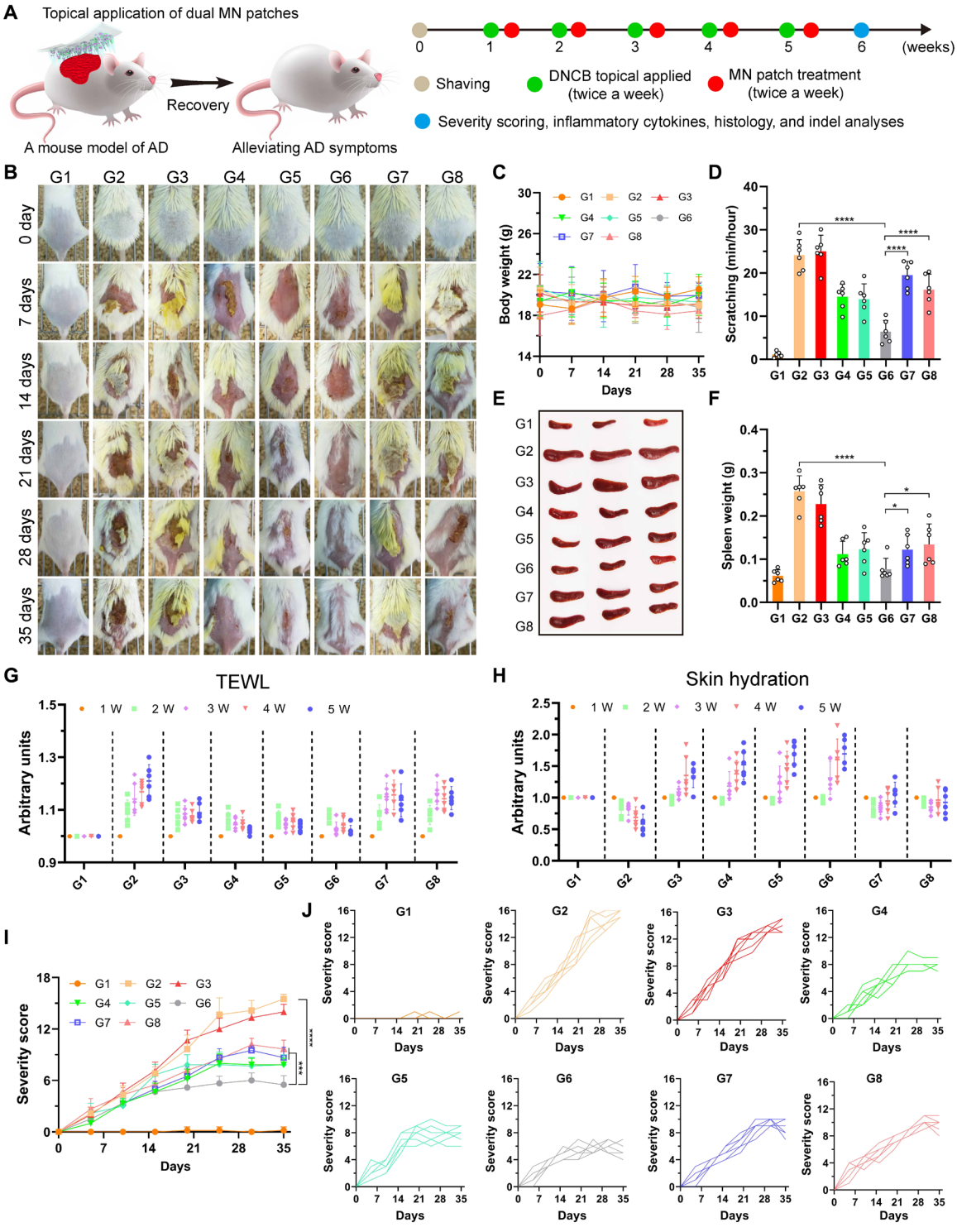


**Fig. 4. Mitigation of DNCB-induced AD via dual MN patch.** (**A**) Schematic illustration of dual MN patch for the treatment of DNCB-induced AD. (**B**) Photographs of mice treated with various formulations. (**C**) The body weight change during the treatment. (**D**) Scratching behaviors during the treatment. (**E**) Representative gross image of the spleens at day 35. (**F**) Spleen weights at day 35. (**G** and **H**) TEWL (G) and skin hydration (H) were examined at weeks 0 to 5 in the various groups. Scores in each mouse at week 0 were arbitrarily set at 1. (**I** and **J**) Dermatitis severity scores were measured once a week for 5 weeks. For (B) to (J), the code denotes the following: G1, normal mice without DNCB treatment; G2, DNCB-treated mice; G3, DNCB-treated mice treated with blank MN patch; G4, DNCB-treated mice treated with Dex-loaded MN patch; G5, DNCB-treated mice treated with RNP-loaded MN patch; G6, DNCB-treated mice treated with dual-loaded MN patch; G7, DNCB-treated mice treated with Dex cream; G8, DNCB-treated mice treated with tacrolimus ointment. Means ± SD, $n = 6$; Student's $t$ test, $^{*}P < 0.05$, $^{***}P < 0.001$, and $^{****}P < 0.0001$. Photo credits: Tao Wan, College of Pharmaceutical Sciences, Zhejiang University.

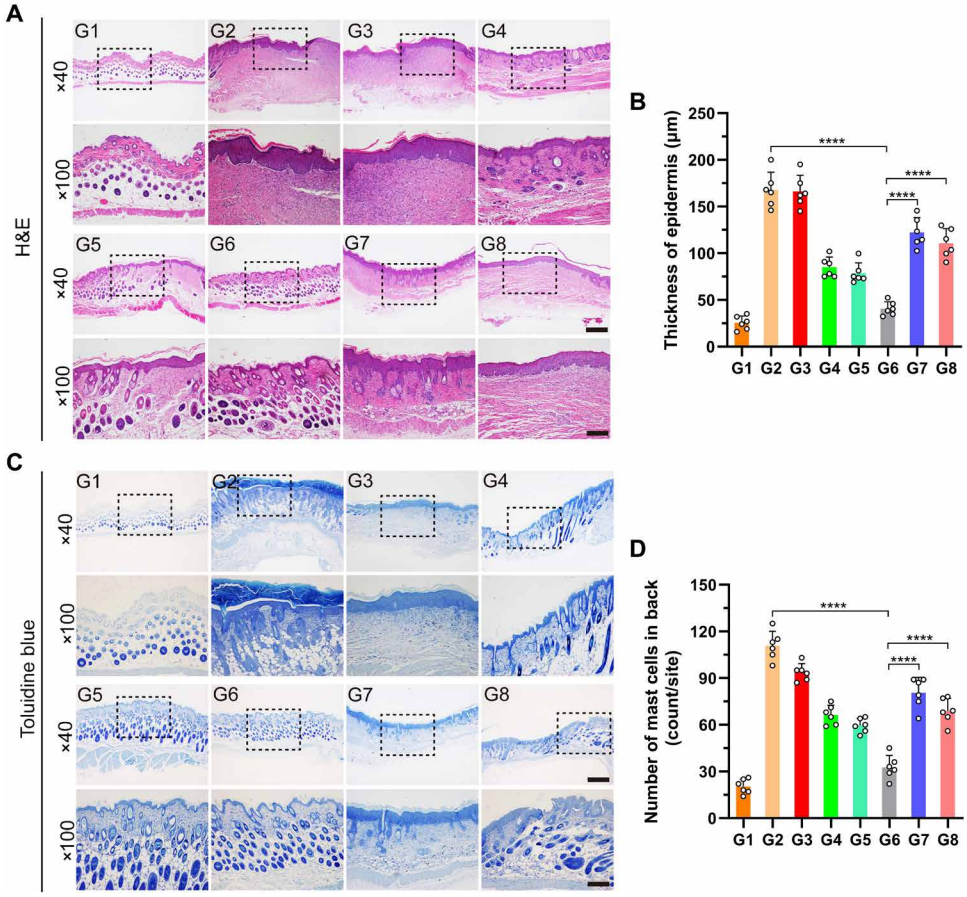


**Fig. 5. Histological analysis of skin tissue sections from AD mice after the specified treatments.** Tissues were prepared for histological analysis, and the sections were stained with H&E staining (**A**) (magnification, ×40 and ×100; scale bars, 500 and 200 μm, respectively) and toluidine blue staining (**C**) (magnification, ×40 and ×100; scale bars, 500 and 200 μm, respectively). Epidermal and dermal thicknesses were measured in H&E-stained microphotographs (**B**), and mast cells were counted in H&E-stained microphotographs (**D**). Error bars represent the SE (means ± SD, $n = 6$). For (A) to (D), the code denotes the following: G1, normal mice without DNCB treatment; G2, DNCB-treated mice; G3, DNCB-treated mice treated with blank MN patch; G4, DNCB-treated mice treated with Dex-loaded MN patch; G5, DNCB-treated mice treated with RNP-loaded MN patch; G6, DNCB-treated mice treated with dual-loaded MN patch; G7, DNCB-treated mice treated with Dex cream; G8, DNCB-treated mice treated with tacrolimus ointment. Means ± SD, $n = 6$; Student's $t$ test, ****$P < 0.0001$.

mutations at the targeted loci, including base deletion, insertion, and substitution around the PAM (Fig. 6A and fig. S15). Deep sequencing analysis of a single library prepared from genomic DNA pooled from mice also indicated significant mutation in *NLRP3* locus, which is consistent with the results of T7E1 assays. The NLRP3 inflammasome activation could result in the cleavage and activation of caspase-1 (*13*), which could further cleave the precursors of interleukin-1β (IL-1β) and IL-18 into mature forms and induce the release of several proinflammatory cytokines, including IL-1β and IL-18 (*13*). To confirm the effectiveness of the MN patch to alleviate the typical symptoms of AD mouse models through Cas9-mediated disruption of the NLRP3 inflammasome, we detected the protein expression of IL-1β, IL-18, and NLRP3 in cutaneous homogenates of mice after different treatments (Fig. 6B and fig. S16). In contrast to other groups, the NLRP3, IL-1β, cleaved caspase-1 p10 (casp-1 p10), and IL-18 in the dorsal cutaneous homogenates remarkably down-regulated following dual MN patch–mediated treatment; however, the expression of IL-1β precursor (pro–IL-1β) and caspase-1 precursor (casp-1 p45) was not affected by other MN treatments, suggesting that targeting NLRP3 inflammasome by means of genome editing would not affect the transcription and the expression of IL-1β and caspase-1 precursor proteins. Furthermore, many patients who suffered from AD, especially those in severe stages, often show IgE-mediated sensitization to common allergens. Thus, serum IgE is regarded as an important indicator of AD. As expected, serum IgE levels significantly down-regulated through dual MN patch–mediated treatment (Fig. 6C). In agreement with Western blot results, the release of IL-1β (Fig. 6D) and IL-18 (Fig. 6E), as determined by ELISA, also significantly decreased in the AD mice that were treated by dual MN patch. In AD lesions, the expression of a number of genes, most of which are related to keratinocyte activity and T cell infiltration, was altered. In particular, genes encoding $T_H2$-type cytokines, including IL-4, IL-10, and IL-13, were found to be up-regulated (*29*). In our study, the expression of IL-4 increased following imiquimod treatment, whereas the treatment by MN patch significantly decreased IL-4 expression (Fig. 6F). During the progression of AD, the disruption of epidermal barriers promotes the inflammation through the dysregulation of immunomodulatory proteins and the release of damage-associated molecular pattern molecules, such as thymic stromal lymphopoietin (TSLP) (*5*). The

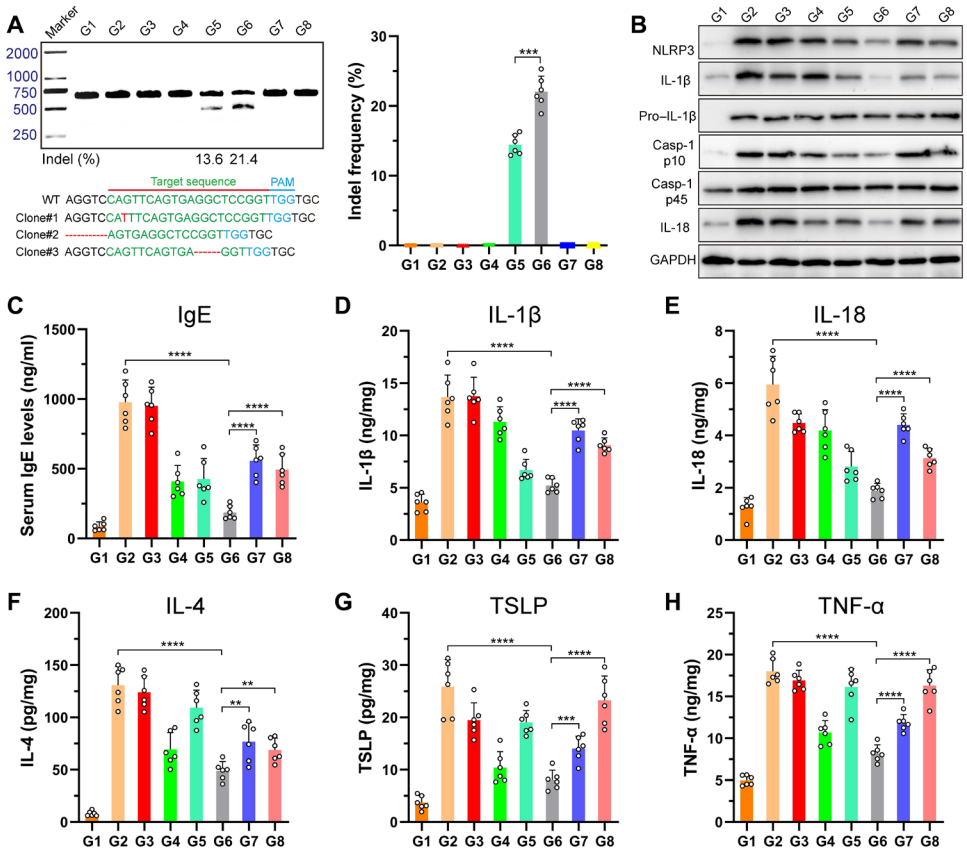


**Fig. 6. Detection of *NLRP3* knockout efficiency and inflammasome-related protein expression in AD mice after the specified treatments.** (**A**) Frequency of indel mutation detected by T7E1 assay from the skin tissues and representative Sanger sequencing results of T-A cloning from the skin tissue after dual MN patch treatment. (**B**) Immunoblot analysis of NLRP3 and other inflammasome protein expression in the dorsal skin homogenates. GAPDH, glyceraldehyde-3-phosphate dehydrogenase. (**C**) Serum IgE levels determined by ELISA. (**D** to **H**) ELISA of IL-1β (D), IL-18 (E), IL-4 (F), TSLP (G), and TNF-α (H) production in the skin tissues of mice treated with various formulations. For (A) to (H), the code denotes the following: G1, normal mice without DNCB treatment; G2, DNCB-treated mice; G3, DNCB-treated mice treated with blank MN patch; G4, DNCB-treated mice treated with Dex-loaded MN patch; G5, DNCB-treated mice treated with RNP-loaded MN patch; G6, DNCB-treated mice treated with dual-loaded MN patch; G7, DNCB-treated mice treated with Dex cream; G8, DNCB-treated mice treated with tacrolimus ointment. Means ± SD, $n = 6$; Student's $t$ test, $^{**}P < 0.01$, $^{***}P < 0.001$, and $^{****}P < 0.0001$.

cytokine level of TSLP in the dorsal skin homogenates remarkably increased following DNCB stimulation, whereas it was down-regulated by topical application of the MN patch (Fig. 6G). Furthermore, the secretion of the proinflammatory cytokine tumor necrosis factor–α (TNF-α) was obviously inhibited following dual MN patch–mediated treatment (Fig. 6H), suggesting the improvement of the overall inflammatory environment in the AD skin tissues. As expected, the dual MN patch–mediated treatment exhibited the strongest inhibition effects against the expression of various immunomodulatory proteins, including IL-1β, IL-18, IL-4, TSLP, and TNF-α, owing to the synergistic anti-inflammatory activity. Collectively, these results indicated that the combination delivery of Dex and RNP through the MN patch could be a promising strategy for treating AD-like skin inflammation.

## Treatment of psoriasis by MN patch

Next, we investigated whether the topical application of MN patch is also effective for the treatment of psoriasis (Fig. 7A). The degree of disease severity was evaluated daily using an objective scoring system based on the Psoriasis Area and Severity Index (PASI), including erythema, scaling, and induration (Fig. 7, G and H). As shown in Fig. 7 (B and C), the repeated topical administration of imiquimod cream on the mouse dorsal skin for consecutive 7 days induced skin lesions such as erythema, scaling, induration, and enhanced skinfold thickness. The application of either Dex-loaded or dual MN patch treatment greatly ameliorated the severity of clinical signs and psoriasis symptoms that were induced by the treatment of imiquimod cream, as compared with the psoriasis mice without any treatment, or by the treatment with an empty MN patch. Compared with MN-mediated monotherapy with either Dex or RNP, the clinically relevant, conventional topical therapies by using Dex cream or tacrolimus ointment generated the unsatisfactory therapeutic effect, as reflected by PASI scores. According to PASI scores, the treatment by dual MN patch exhibited the strongest anti-inflammatory effects. No obvious change in body weight was monitored during the treatment period, implying the safe profile of the dual MN patch (Fig. 7D). It has been previously reported that imiquimod could induce a significant enlargement of the spleen with a weight increase, attributed to the release of inflammatory cytokines (*30*, *31*). As expected, whereas the size and weight of the spleen increased in the imiquimod-treated mice, the spleen of the MN patch–treated mice showed a similar spleen weight and size to that of the normal group

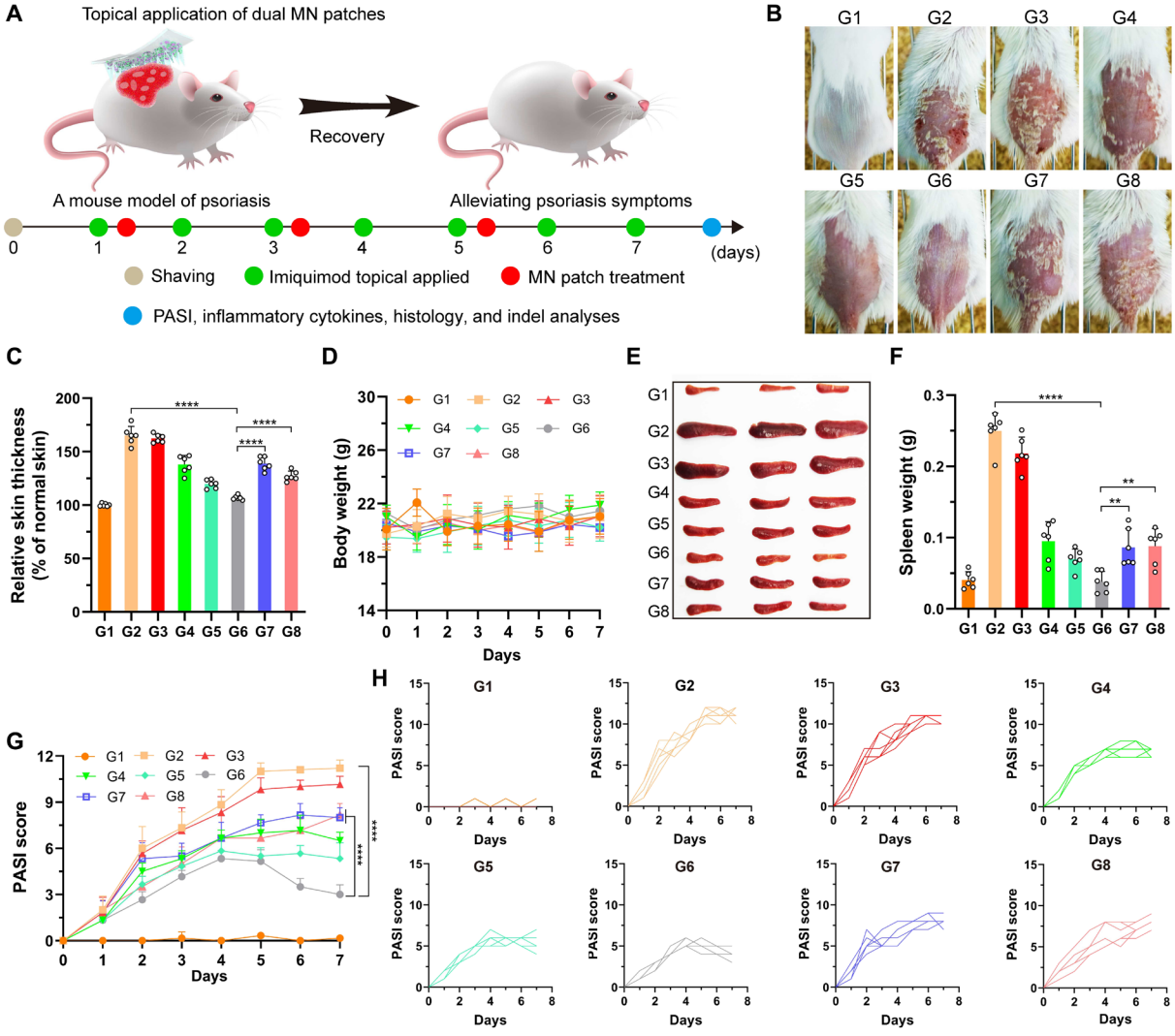


**Fig. 7. Mitigation of imiquimod-induced psoriasis via dual MN patch.** (**A**) Schematic illustration of dual MN patch for the treatment of imiquimod-induced psoriasis. (**B**) Photographs of mice treated with various formulations. (**C**) Back skinfold thickness of various groups. Skinfold thickness is expressed as a percentage relative to that in disease-free control mice. (**D**) The body weight change during the treatment. (**E**) Representative gross image of the spleens at day 8. (**F**) Spleen weights at day 8. (**G** and **H**) PASI scores were measured every day for 1 week. For (B) to (H), the code denotes the following: G1, normal mice without imiquimod treatment; G2, imiquimod-treated mice without therapy; G3, imiquimod-treated mice treated with blank MN patch; G4, DNCB-treated mice treated with Dex-loaded MN patch; G5, imiquimod-treated mice treated with RNP-loaded MN patch; G6, imiquimod-treated mice treated with dual-loaded MN patch; G7, imiquimod-treated mice treated with Dex cream; G8, imiquimod-treated mice treated with tacrolimus ointment. Means ± SD, $n = 6$; Student's $t$ test, $^{**}P < 0.01$ and $^{****}P < 0.0001$. Photo credits: Tao Wan, College of Pharmaceutical Sciences, Zhejiang University.

(Fig. 7, E and F). As documented previously, psoriasis is generally characterized by epidermal hyperplasia, a result of hyperproliferation and aberrant differentiation of keratinocytes and massive infiltration of inflammatory immune cells (*32*, *33*). Furthermore, in agreement with the above findings, the histological analysis of the punch biopsy specimens from the treated back skin implied a considerable decrease in terms of epidermal hyperplasia and inflammatory cell infiltration, as compared with mice by MN patch–mediated monotherapy (Fig. 8H and fig. S17). These findings were further supported by the reduced weight of punch biopsy specimens (fig. S18), suggesting the alleviation in skin edema after dual MN patch–mediated treatment.

Last, we detected the indel frequency of *NLRP3* genomic locus by T7E1 assay. Similar to the findings in the treatment of AD, whereas the indel frequency induced by RNP-loaded MN patch was 10.7% (Fig. 8A), dual MN patch–mediated treatment significantly improved the indel frequency up to 17.2%, suggesting the critical role of Dex in promoting genome-editing activity in vivo. The representative sequences of indels in the *NLRP3* locus of dual-loaded MN patch–treated mice are shown in Fig. 8A. Deep sequencing analysis of a single library prepared from genomic DNA pooled from mice also indicated substantial mutation in the *NLRP3* locus, which is consistent with the results of the T7E1 assay (fig. S19). To further confirm whether dual MN patch–mediated treatment could inhibit the activation of the NLRP3 inflammasome in vivo, we detected the expression of IL-1β, pro–IL-1β, IL-18, and NLRP3 in skin homogenates (Fig. 8B and fig. S20). Compared with psoriasis mice without any treatment, IL-1β and IL-18 secretion in skin homogenates reduced significantly after the dual MN patch–mediated treatment. Among various treatments, the most obvious inhibitory effect on IL-1β and

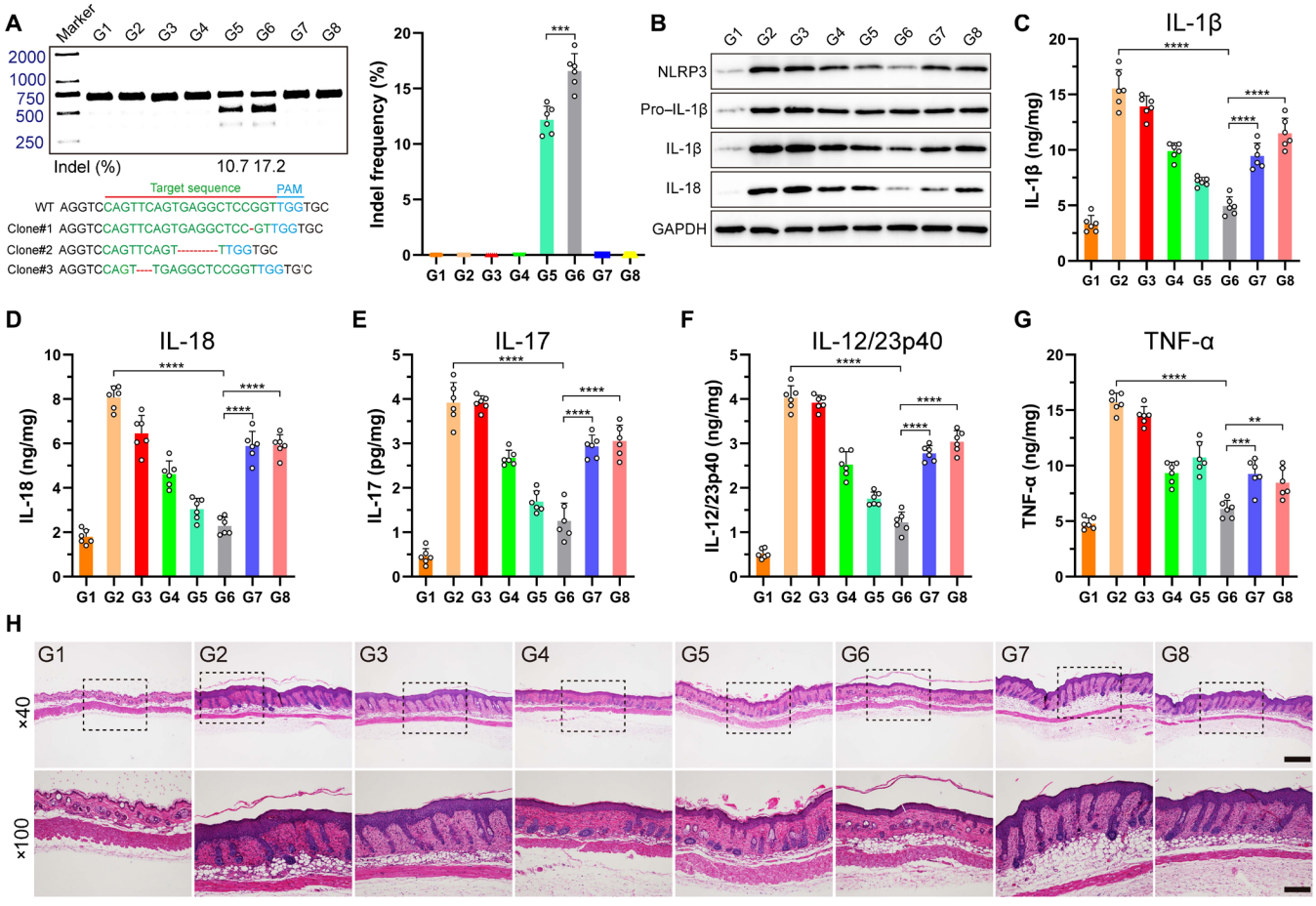


**Fig. 8. Detection of *NLRP3* knockout efficiency and inflammasome-related protein expression in psoriasis mice after the specified treatments.** (**A**) Frequency of indel mutation detected by T7E1 assay from the skin tissues and representative Sanger sequencing results of T-A cloning from the skin tissue after dual MN patch treatment. (**B**) Immunoblot analysis of NLRP3 and other inflammasome protein expression in the dorsal skin homogenates. (**C** to **G**) ELISA of IL-1β (C), IL-18 (D), IL-17 (E), IL-12/23p40 (F), and TNF-α (G) production in the skin tissues of mice treated with various formulations. (**H**) H&E staining of the skin tissue sections from the mice after the specified treatments (magnification, ×40 and ×100; scale bars, 500 and 200 μm, respectively). For (A) to (H), the code denotes the following: G1, normal mice without imiquimod treatment; G2, imiquimod-treated mice without therapy; G3, imiquimod-treated mice treated with blank MN patch; G4, DNCB-treated mice treated with Dex-loaded MN patch; G5, imiquimod-treated mice treated with RNP-loaded MN patch; G6, imiquimod-treated mice treated with dual-loaded MN patch; G7, imiquimod-treated mice treated with Dex cream; and G8, imiquimod-treated mice treated with tacrolimus ointment. Means ± SD, $n = 6$; Student's $t$ test, $^{**}P < 0.01$, $^{***}P < 0.001$, and $^{****}P < 0.0001$.

IL-18 secretion was observed over the dual MN patch–treated mice, indicating the effective inhibition of NLRP3 inflammasome activation. The expression of pro–IL-1β, however, was not affected by any of these treatments. Furthermore, we measured the release of IL-1β, IL-18, IL-17, IL-12/23p40, and TNF-α with ELISA results, which revealed that the production of IL-1β (Fig. 8C) and IL-18 (Fig. 8D) in the skin was significantly inhibited by MN-mediated monotherapy or the combination treatment, which are all in agreement with the Western blot results. Moreover, T cell signaling is essential in understanding the pathogenesis, treatment, and comorbidities associated with psoriasis, and multiple T cell lineages—including $T_H1$, $T_H2$, $T_H17$, and $T_H22$—and regulatory T cells (*3*) have been described in correlation to the progression of psoriasis. Each T cell lineage produces its own signature cytokines and processes signals through a set of transcriptional factors. At the most rudimentary level, $T_H1$ cells are associated with IL-12/23p40 and $T_H17$ cells with IL-17, whereas TNF-α is not specific to a single $T_H$ cell profile. Thus, we determined the expression of the key psoriasis-related cytokines in skin lesions, including TNF-α, IL-17, and IL-12/23p40. Protein levels of the psoriasis-related cytokines IL-17 (Fig. 8E), IL-12/23p40 (Fig. 8F), and TNF-α (Fig. 8G) in skin homogenates significantly reduced after the dual MN patch–mediated therapy. These results suggest that topical treatment of dual MN patch could effectively ameliorate psoriasis-like skin inflammation. Furthermore, we performed deep sequencing analysis to quantify the degree of off-target mutations in vivo. The potential off-target loci were determined using Cas-OFFinder (www.rgenome.net/cas-offinder/), as listed in table S3. Target genes were amplified first with primer sets and then amplified again with the deep sequencing primers listed in table S4. As shown in figs. S21 and S22 and table S5, five predicted off-target sites (off3, off4, off5, off6, and off8) were found to be minimal and similar to the levels of sequencing error (0.005 to 0.2%). However, detectable off-target mutations were found in the three predicted off-target sites (off1, off2, and off7). Collectively, MN patch–mediated genome editing toward *NLRP3* in combination with glucocorticoid therapy has been demonstrated to be effective in treating ISDs, as

we have shown in the current studies for treating AD and psoriasis as proof-of-concept therapeutic examples.

## DISCUSSION

Both psoriasis and AD belong to chronic ISDs and are often clinically manifested by intensive itch, excessive scratching, redness, and impairment of epidermal barrier function. These manifestations can lead to extreme discomfort, sleep deprivation, and diminished self-esteem (*3*, *5*). During the development and progression of both ISDs, the abnormal activation of immune responses is commonly characterized as a result of the aberrant differentiation of keratinocytes, the massive infiltration of inflammatory immune-related cells, and the increased release of proinflammatory cytokines in both dermis and epidermis involving the innate and adaptive immune systems (*3*, *5*, *34*, *35*). Among various treatment options, topical administration of glucocorticoids is widely endorsed as the first-line anti-inflammatory treatment in patients with AD or psoriasis. However, most patients often show poor response to glucocorticoid therapy in the long-term treatment, largely due to glucocorticoid resistance. The current MN-mediated therapeutic strategy takes advantage of the CRISPR-Cas9–based genome editing technology that can down-regulate NLRP3 expression by precisely targeting the genomic locus of *NLRP3*, which has been demonstrated not only to alleviate the typical symptoms of ISDs by deactivating various abnormal innate and adaptive immune responses but also to decrease glucocorticoid resistance in immune-related cells to improve glucocorticoid sensitivity. Acute ISDs, such as urticaria and ultraviolet B–induced damage, also involve the functional mutation of *NLRP3* or the activation of NLRP3 inflammasomes within subcutaneous keratinocytes and mast cells. As a result, MN-assisted subcutaneous genome editing by targeting NLRP3 inflammasomes may also contribute to glucocorticoid therapy and can be extended to the treatment of acute ISDs as well (*10*). Note that MN-mediated treatment combines a stepwise delivery strategy where MN first enables the efficient transdermal delivery of Dex-loaded PLGA nanoparticles and polymer/Cas9 nanocomplexes into inflammatory epidermal and dermal layers, where these nanoparticles can further transport Cas9 and Dex into cell nuclei to exert their respective functions. Such a stepwise delivery strategy well circumvents the barriers at both transdermal and intracellular levels, thereby maximizing the therapeutic effects of synergistic therapy. As expected, MN-assisted genome editing greatly improves glucocorticoid therapy, which is superior to the treatment by clinically available Dex cream or tacrolimus ointment. As a painless, user-friendly administration approach, further optimization of the MN patch is still essential to accelerate its future clinical translation.

## MATERIALS AND METHODS

### Materials

DNCB was obtained from Sigma-Aldrich (St. Louis, MO). Imiquimod cream [5 weight % (wt %)] was purchased from 3M Pharmaceuticals (Aldara; Leicestershire, UK). Dex cream was purchased from CR Sanjiu (Shenzhen, China). Tacrolimus ointment was purchased from Astellas (Toyama, Japan). Penicillin-streptomycin, PBS, and fetal bovine serum (FBS) were purchased from Thermo Fisher Scientific (USA). HA was obtained from Bloomage Freda Biopharm Co. Ltd. (Shandong, China). CTP was supplied by Jellice Co. Ltd. (Miyagi, Japan). CRISPR-Cas9 protein was purchased from GenScript (Nanjing, China). T7E1 enzyme was obtained from New England Biolabs (Beijing, China). Lipofectamine CMAX Transfection Reagent was bought from Thermo Fisher Scientific (Germany). sgNLRP3 was designed by online tools (http://crispr.mit.edu/ and http://chopchop.cbu.uib.no/) and then prepared using the HiScribe T7 Quick High Yield RNA Synthesis Kit (New England Biolabs, MA, USA). Primers for in vitro transcription of gRNAs are listed in table S1. Primary antibodies used in this project included the following: Anti-NLRP3 (1:1000; ER1706-72) antibody was obtained from HUABIO (Hangzhou, China), anti–caspase-1 p10 (1:1000; sc-514) and anti–glyceraldehyde-3-phosphate dehydrogenase antibodies were obtained from Santa Cruz Biotechnology (CA, USA), and anti–IL-1β (1:1000; ab200478) was obtained from Abcam (Shanghai, China).

### Characterization of PLGA/Dex nanoparticles and CP/Ad-SS-GD/RNP nanoparticles

PLGA/Dex nanoparticles were prepared via an emulsion/solvent evaporation method. Briefly, 10 mg of PLGA and 1 mg of Dex were dissolved in 0.8 ml of dichloromethane, followed by an addition of 2 ml of 3% poly(vinyl alcohol) (PVA) solution. Subsequently, the mixture solution was sonicated and dispersed into 8 ml of 0.3% PVA solution under stirring. Last, the solution was applied to the rotary evaporator for dichloromethane evaporation. RNP-loaded CP/Ad-SS-GD nanocomplexes were prepared as our previous paper described (*18*). The average particle size and zeta potential of the nanoparticles were measured by DLS analysis using a Zetasizer (Nano ZS90, Malvern Instruments, Worcestershire, UK). The morphological characteristic of the nanocomplexes was characterized by TEM (JEM1400, Tokyo, Japan).

### Preparation of the MN patch

The fabrication of the MN patch was performed using a silicone micromold with each needle cavity being a 200 μm–by–200 μm quadrangular base tapering to a height of 600 μm. The MNs were arranged in a 15-by-15 array with a 500-μm center-to-center spacing. For the preparation of the MN patch, first, 10 wt % HA solution containing CTP (from 0 to 30 wt %), Cas9 protein–loaded CP/Ad-SS-GD nanoparticles, and Dex-loaded PLGA nanoparticles was deposited into the needle cavities then dried under vacuum for 15 min. Next, 100 μl of HA and CTP solution was deposited to fill the needle cavities, followed by removal of the excessive solution. This micromold was stored in a dry place overnight at room temperature to form an HA-CTP hydrogel. The loading capacities of Cas9 protein and Dex were 20 and 60 μg, respectively, in the MNs. Subsequently, 500 μl of HA solution was deposited onto the MN and kept under air for 4 hours at 25°C. After complete desiccation, the MN patch was detached from the micromold. The morphology of the MNs was characterized by SEM. The fluorescent MNs were fabricated with PLGA/rhodamine B and CP/Ad-SS-GD/Cas9 protein–FITC nanoparticles. Cas9 protein was labeled with FITC as previously described (*36*). The fluorescence images of MNs were taken by an Olympus IX70 multiparameter fluorescence microscope.

### In vitro release study

For the in vitro release of Cas9 protein or Dex, the needle tips of the MN patch were immersed in the PBS solution containing glutathione at 37°C. At a predetermined time point, the PBS solution was collected and replaced with an equivalent volume of fresh PBS. The concentration of Dex and protein in the PBS solution was determined

with the standard bicinchoninic acid assay and high-performance liquid chromatography, respectively. The released percentage of Cas9 protein or Dex was recorded at each time point by taking the loading amount of Cas9 protein or Dex in the MNs as 100%.

### In vivo degradation study of the MN patch

To investigate the in vivo degradation of the MN patch, the fluorescent MNs were fabricated with PLGA/rhodamine B and CP/Ad-SS-GD/Cas9 protein–FITC nanoparticles. In this test, the MN patch was inserted into the shaved mouse skin. Skin tissue samples were embedded in an optical cutting temperature compound (Sakura Finetek, USA) for frozen sectioning. The specimens were sliced into sections with a thickness of 20 μm, and the skin slice was observed using confocal laser scanning microscopy (Carl Zeiss 880, Germany).

### *NLRP3* gene disruption assay

NIH/3T3 cells and DC2.4 cells were purchased from the American Type Culture Collection. The 3T3 cells and DC2.4 cells were cultured in Dulbecco's modified Eagle's medium containing 10% FBS at 37°C under 5% $CO_2$. After different concentrations of Dex-loaded PLGA nanoparticle treatment, the cell was transfected with polymer/RNP nanocomplexes. The doses of protein, sgRNA, and polymer in each well were 1, 0.5, and 8 μg, respectively. After incubation for 6 hours, the culture media containing transfection mixtures were removed and further incubated for 42 hours.

### DNCB-induced AD mouse model and in vivo treatment

Male BALB/c mice (6 to 8 weeks old) were housed in a room controlled for temperature (23° ± 3°C) and relative humidity (40 to 60%). All animal treatments or procedures were carried out in accordance with the guidelines of the Laboratory Animal Welfare and Ethics Committee of Zhejiang University. The mice were shaved before in vivo therapy experiment. AD was induced by topical stimulation with 1% DNCB (200 μl of a 2:1 mixture of acetone/olive oil) in the delimited area of the back skin every 2 days at the first week. Then, 0.5% DNCB was repeated three times a week orderly for 4 weeks. Different types of MN patch per mice were topically applied twice a week for 5 weeks. The MN patch was pressed firmly for 60 s to penetrate through the stratum corneum and epidermis and then pressed softly for an additional 30 s to make the patch absorb the liquid in the skin. The MN patch was further fixed using medical tape for further sustained drug release. Dex cream and tacrolimus ointment per mice per day were topically applied for 5 weeks. Normal mice without any treatment were not stimulated by DNCB. During the treatment, the AD severity score was recorded as the sum of scores graded as 0 (no symptoms), 1 (mild), 2 (moderate), 3 (severe), or 4 (very serve) for each of the four measured symptoms (erythema/hemorrhage, excoriation/erosion, edema, and scarring/dryness). TEWL was determined with a Tewameter TM 210 to assess skin barrier disruption. Skin hydration was measured with a Corneometer CM 820 in arbitrary units. Both TEWL and skin hydration were measured on days 0, 7, 14, 21, 28, and 35 before the application of DNCB. Scratching behavior of AD mice was recorded by video and then analyzed by playing back the video. Before observation of scratching, AD mice were acclimatized for a minimum of 45 min in an observation chamber. The cumulative duration of scratching behavior in 1 hour was calculated. After 5 weeks, mice were sacrificed to obtain skin tissues, spleen, and blood. Back skinfold thickness was measured using a micrometer (Mitutoyo Corporation, Mitsutomo, Japan). In the histologic analysis, the skin was fixed in 4% paraformaldehyde and stained with hematoxylin and eosin (H&E) and toluidine blue for microscopic observation.

### Imiquimod-induced psoriasis mouse model and in vivo treatment

Mice were topically administrated daily at a dose of 100 mg of 5% imiquimod cream on the shaved region of their back for seven consecutive days. Normal mice without any treatment were not stimulated by imiquimod cream. Two hours after imiquimod cream application, different types of MN patch per mice were topically applied on delimited back skin. The MN patch was pressed firmly for 60 s to penetrate through the stratum corneum and epidermis, and then the MN patch was pressed softly for an additional 30 s to make the patch absorb the liquid in the skin. The MN patch was further fixed using medical tape for further sustained drug release. Dex cream and tacrolimus ointment per mice per day were topically applied for 6 days. During the treatment, the PASI score was recorded as the sum of scores graded as 0 (no symptoms), 1 (mild), 2 (moderate), 3 (severe), or 4 (very serve) for each of the three measured symptoms (erythema, scaling, and induration). Erythema was graded using a scoring table with red tints. After 7 days, mice were sacrificed to obtain skin tissues and spleen. In the histologic analysis, the skin was fixed in 4% paraformaldehyde and stained with H&E for microscopic observation.

### T7E1 assay and Sanger sequencing

Genomic DNA of cells or skin tissues was extracted using the QIAGEN DNeasy Blood & Tissue Kit following the manufacturer's protocol. The flanking region of the *NLRP3* targeting sequence was amplified by polymerase chain reaction (PCR) (primers for PCR amplification are listed in table S2). Two hundred nanograms of purified PCR products was used to perform T7E1 assay. The fragmented PCR products were analyzed with 1% agarose gel electrophoresis and imaged with a gel documentation system (c150, Azure Biosystems, USA). The percentage of nuclease-specific digested products was calculated by ImageJ. The indel frequency was calculated with the following formula: $100 \times (1 - (1 - \text{fraction cleaved})^{1/2})$, where fraction cleaved equals the percentage of nuclease-specific cleavage products. The PCR products of the genomic region–flanking target sites of *NLRP3* locus were cloned into the T clone vector for Sanger sequencing.

### Deep sequencing and off-target analysis

The fragmented PCR products were quantified using deep sequencing assay, and a library of genomic DNA pooled from the sample in triplicate was subjected to deep sequencing analysis using CRISPResso2 (http://crispresso.pinellolab.partners.org/). Potential off-target loci were determined using Cas-OFFinder (www.rgenome.net/cas-offinder/). All the off-target sites and primers for PCR amplification are listed in tables S3 and S4. Off-target analysis procedure was similar to the on-target examination through Sanger sequencing.

### Western blot

Total protein from the skin samples was extracted using radioimmunoprecipitation assay lysis buffer. All protein lysates were separated by 10% SDS–polyacrylamide gel electrophoresis and transferred onto polyvinylidene difluoride membranes using a wet-transfer system. The membranes were blocked in tris-buffered saline with Tween

(TBST) buffer containing 5% bovine serum albumin for 1 hour and then were incubated with primary antibodies diluted in TBST buffer overnight at 4°C.

### Enzyme-linked immunosorbent assay

For determination of serum IgE levels, blood was collected in serum separator tubes. Serum was separated by centrifugation (3000 rpm, 15 min, 4°C) and stored at −80°C for further use. Serum IgE level was determined with a mouse IgE ELISA quantification kit from Solarbio (Beijing, China) following the manufacturer's protocol. An optical density was measured at 450-nm wavelength. Inflammatory cytokines in supernatants of skin homogenates were determined using ELISA kits (MultiSciences, China), as indicated above.

### Statistical analysis

All data and figures in this paper were analyzed and plotted by GraphPad Prism 8.0. The obtained data are expressed as means ± SD. Biological replicates were used in all experiments unless otherwise stated. The statistical significance was analyzed using Student's *t* test. A *P* value less than 0.05 was considered significant (*$P < 0.05$, **$P < 0.01$, ***$P < 0.001$, and ****$P < 0.0001$).

## SUPPLEMENTARY MATERIALS

Supplementary material for this article is available at http://advances.sciencemag.org/cgi/content/full/7/11/eabe2888/DC1

View/request a protocol for this paper from *Bio-protocol*.

## REFERENCES AND NOTES


1. G. Girolomoni, Classifying immunopathological responses in chronic inflammatory skin diseases. *J. Eur. Acad. Dermatol. Venereol.* **32**, 654–655 (2018).
2. F. O. Nestle, D. H. Kaplan, J. Barker, Psoriasis. *N. Engl. J. Med.* **361**, 496–509 (2009).
3. J. E. Greb, A. M. Goldminz, J. T. Elder, M. G. Lebwohl, D. D. Gladman, J. J. Wu, N. N. Mehta, A. Y. Finlay, A. B. Gottlieb, Psoriasis. *Nat. Rev. Dis. Prim.* **2**, 16082 (2016).
4. T. Bieber, Atopic dermatitis. *N. Engl. J. Med.* **358**, 1483–1494 (2008).
5. S. Weidinger, L. A. Beck, T. Bieber, K. Kabashima, A. D. Irvine, Atopic dermatitis. *Nat. Rev. Dis. Prim.* **4**, 1 (2018).
6. K. Welsch, J. Holstein, A. Laurence, K. Ghoreschi, Targeting JAK/STAT signalling in inflammatory skin diseases with small molecule inhibitors. *Eur. J. Immunol.* **47**, 1096–1107 (2017).
7. P. Broz, V. M. Dixit, Inflammasomes: Mechanism of assembly, regulation and signalling. *Nat. Rev. Immunol.* **16**, 407–420 (2016).
8. D. C. de Sá, C. Festa Neto, Inflammasomes and dermatology. *An. Bras. Dermatol.* **91**, 566–578 (2016).
9. Y. Xiao, W. Xu, W. Su, NLRP3 inflammasome: A likely target for the treatment of allergic diseases. *Clin. Exp. Allergy* **48**, 1080–1091 (2018).
10. D. Wang, B. Duncan, X. Li, J. Shi, The role of NLRP3 inflammasome in infection-related, immune-mediated and autoimmune skin diseases. *J. Dermatol. Sci.* **98**, 146–151 (2020).
11. S. W. Paugh, E. J. Bonten, D. Savic, L. B. Ramsey, W. E. Thierfelder, P. Gurung, R. K. S. Malireddi, M. Actis, A. Mayasundari, J. Min, D. R. Coss, L. T. Laudermilk, J. C. Panetta, J. R. McCorkle, Y. Fan, K. R. Crews, G. Stocco, M. R. Wilkinson, A. M. Ferreira, C. Cheng, W. Yang, S. E. Karol, C. A. Fernandez, B. Diouf, C. Smith, J. K. Hicks, A. Zanut, A. Giordanengo, D. Crona, J. J. Bianchi, L. Holmfeldt, C. G. Mullighan, M. L. den Boer, R. Pieters, S. Jeha, T. L. Dunwell, F. Latif, D. Bhojwani, W. L. Carroll, C.-H. Pui, R. M. Myers, R. K. Guy, T.-D. Kanneganti, M. V. Relling, W. E. Evans, NALP3 inflammasome upregulation and CASP1 cleavage of the glucocorticoid receptor cause glucocorticoid resistance in leukemia cells. *Nat. Genet.* **47**, 607–614 (2015).
12. S. W. Paugh, E. J. Bonten, W. E. Evans, Inflammasome-mediated glucocorticoid resistance: The receptor rheostat. *Mol. Cell. Oncol.* **3**, e1065947 (2015).
13. B.-Z. Shao, Z.-Q. Xu, B.-Z. Han, D.-F. Su, C. Liu, NLRP3 inflammasome and its inhibitors: A review. *Front. Pharmacol.* **6**, 262 (2015).
14. G. Deng, W. Chen, P. Wang, T. Zhan, W. Zheng, Z. Gu, X. Wang, X. Ji, Y. Sun, Inhibition of NLRP3 inflammasome-mediated pyroptosis in macrophage by cycloastragenol contributes to amelioration of imiquimod-induced psoriasis-like skin inflammation in mice. *Int. Immunopharmacol.* **74**, 105682 (2019).
15. M. J. Primiano, B. A. Lefker, M. R. Bowman, A. G. Bree, C. Hubeau, P. D. Bonin, M. Mangan, K. Dower, B. G. Monks, L. Cushing, S. Wang, J. Guzova, A. Jiao, L.-L. Lin, E. Latz, D. Hepworth, J. P. Hall, Efficacy and pharmacology of the NLRP3 inflammasome inhibitor CP-456,773 (CRID3) in murine models of dermal and pulmonary inflammation. *J. Immunol.* **197**, 2421–2433 (2016).
16. H. Jiang, H. He, Y. Chen, W. Huang, J. Cheng, J. Ye, A. Wang, J. Tao, C. Wang, Q. Liu, T. Jin, W. Jiang, X. Deng, R. Zhou, Identification of a selective and direct NLRP3 inhibitor to treat inflammatory disorders. *J. Exp. Med.* **214**, 3219–3238 (2017).
17. C. Xu, Z. Lu, Y. Luo, Y. Liu, Z. Cao, S. Shen, H. Li, J. Liu, K. Chen, Z. Chen, X. Yang, Z. Gu, J. Wang, Targeting of NLRP3 inflammasome with gene editing for the amelioration of inflammatory diseases. *Nat. Commun.* **9**, 4092 (2018).
18. T. Wan, Y. Chen, Q. Pan, X. Xu, Y. Kang, X. Gao, F. Huang, C. Wu, Y. Ping, Genome editing of mutant KRAS through supramolecular polymer-mediated delivery of Cas9 ribonucleoprotein for colorectal cancer therapy. *J. Control. Release* **322**, 236–247 (2020).
19. H. Wang, Y. Li, H. Bai, J. Shen, X. Chen, Y. Ping, G. Tang, A cooperative dimensional strategy for enhanced nucleus-targeted delivery of anticancer drugs. *Adv. Funct. Mater.* **27**, 1700339 (2017).
20. A. Hakuta, Y. Yamaguchi, T. Okawa, S. Yamamoto, Y. Sakai, M. Aihara, Anti-inflammatory effect of collagen tripeptide in atopic dermatitis. *J. Dermatol. Sci.* **88**, 357–364 (2017).
21. G. Yang, Q. Chen, D. Wen, Z. Chen, J. Wang, G. Chen, Z. Wang, X. Zhang, Y. Zhang, Q. Hu, L. Zhang, Z. Gu, A therapeutic microneedle patch made from hair-derived keratin for promoting hair regrowth. *ACS Nano* **13**, 4354–4360 (2019).
22. H. X. Wang, M. Li, C. M. Lee, S. Chakraborty, H. W. Kim, G. Bao, K. W. Leong, CRISPR/Cas9-based genome editing for disease modeling and therapy: Challenges and opportunities for nonviral delivery. *Chem. Rev.* **117**, 9874–9906 (2017).
23. M. Fujii, K. Takeuchi, Y. Umehara, M. Takeuchi, T. Nakayama, S. Ohgami, E. Asano, T. Nabe, S. Ohya, Barbiturates enhance itch-associated scratching in atopic dermatitis mice: A possible clue to understanding nocturnal pruritus in atopic dermatitis. *Eur. J. Pharmacol.* **836**, 57–66 (2018).
24. H.-Y. Song, W. S. Kim, S. Mushtaq, J. M. Park, S.-H. Choi, J.-W. Cho, S.-T. Lim, E.-B. Byun, A novel chrysin derivative produced by gamma irradiation attenuates 2,4-dinitrochlorobenzene-induced atopic dermatitis-like skin lesions in Balb/c mice. *Food Chem. Toxicol.* **128**, 223–232 (2019).
25. H. Ibaraki, T. Kanazawa, Y. Takashima, H. Okada, Y. Seta, Transdermal anti-nuclear kappaB siRNA therapy for atopic dermatitis using a combination of two kinds of functional oligopeptide. *Int. J. Pharm.* **542**, 213–220 (2018).
26. Y. Wang, S. Cao, K. Yu, F. Yang, X. Yu, Y. Zhai, C. Wu, Y. Xu, Integrating tacrolimus into eutectic oil-based microemulsion for atopic dermatitis: Simultaneously enhancing percutaneous delivery and treatment efficacy with relieving side effects. *Int. J. Nanomedicine* **14**, 5849–5863 (2019).
27. A. M. Moreno, N. Palmer, F. Alemán, G. Chen, A. Pla, N. Jiang, W. Leong Chew, M. Law, P. Mali, Immune-orthogonal orthologues of AAV capsids and of Cas9 circumvent the immune response to the administration of gene therapy. *Nat. Biomed. Eng.* **3**, 806–816 (2019).
28. A. Li, M. R. Tanner, C. M. Lee, A. E. Hurley, M. De Giorgi, K. E. Jarrett, T. H. Davis, A. M. Doerfler, G. Bao, C. Beeton, W. R. Lagor, AAV-CRISPR gene editing is negated by pre-existing immunity to Cas9. *Mol. Ther.* **28**, 1432–1441 (2020).
29. G. Yang, H. E. Lee, S. W. Shin, S. H. Um, J. D. Lee, K.-B. Kim, H. C. Kang, Y.-Y. Cho, H. S. Lee, J. Y. Lee, Efficient transdermal delivery of DNA nanostructures alleviates atopic dermatitis symptoms in NC/Nga mice. *Adv. Funct. Mater.* **28**, 1801918 (2018).
30. J. Y. Kim, J. Ahn, J. Kim, M. Choi, H. Jeon, K. Choe, D. Y. Lee, P. Kim, S. Jon, Nanoparticle-assisted transcutaneous delivery of a signal transducer and activator of transcription 3-inhibiting peptide ameliorates psoriasis-like skin inflammation. *ACS Nano* **12**, 6904–6916 (2018).
31. I. Dolz-Pérez, M. A. Sallam, E. Masiá, D. Morelló-Bolumar, M. D. Pérez del Caz, P. Graff, D. Abdelmonsif, S. Hedtrich, V. J. Nebot, M. J. Vicent, Polypeptide-corticosteroid conjugates as a topical treatment approach to psoriasis. *J. Control. Release* **318**, 210–222 (2020).
32. M. Sala, A. Elaissari, H. Fessi, Advances in psoriasis physiopathology and treatments: Up to date of mechanistic insights and perspectives of novel therapies based on innovative skin drug delivery systems (ISDDS). *J. Control. Release* **239**, 182–202 (2016).
33. H. Liang, Y. Yan, J. Wu, X. Ge, L. Wei, L. Liu, Y. Chen, Topical nanoparticles interfering with the DNA-LL37 complex to alleviate psoriatic inflammation in mice and monkeys. *Sci. Adv.* **6**, eabb5274 (2020).
34. C. M. Nguyen, W. Liao, Genomic imprinting in psoriasis and atopic dermatitis: A review. *J. Dermatol. Sci.* **80**, 89–93 (2015).
35. T. Miyagaki, M. Sugaya, Recent advances in atopic dermatitis and psoriasis: Genetic background, barrier function, and therapeutic targets. *J. Dermatol. Sci.* **78**, 89–94 (2015).
36. C. Liu, T. Wan, H. Wang, S. Zhang, Y. Ping, Y. Cheng, A boronic acid–rich dendrimer with robust and unprecedented efficiency for cytosolic protein delivery and CRISPR-Cas9 gene editing. *Sci. Adv.* **5**, eaaw8922 (2019).

**Acknowledgments**
**Funding:** This work was supported by the National Natural Science Foundation of China (82073779 and 81872807), Natural Science Foundation of Zhejiang Province (Distinguished Young Scholar Program, LR21H300002), National Key Research and Development Program of China (2018YFA0901800), Fundamental Research Funds for the Central Universities (2018XZZX001-14), and Leading Talent of "Ten Thousand Plan"—National High-Level Talents Special Support Plan. **Author contributions:** Y.P. conceived the project and designed the experiments. T.W. and Q.P. performed all the experiments. T.W. analyzed the data. Y.P. supervised the project and wrote the manuscript. **Competing interests:** Y.P., T.W., and Q.P. are inventors on a patent application related to this work filed by Zhejiang University (no. 202011131624.6, filed on 21 November 2020). The authors declare that they have no other competing interests. **Data and materials availability:** All data needed to evaluate the conclusions in the paper are present in the paper and/or the Supplementary Materials. Additional data related to this paper may be requested from the authors.

Submitted 22 September 2020
Accepted 26 January 2021
Published 10 March 2021
10.1126/sciadv.abe2888

**Citation:** T. Wan, Q. Pan, Y. Ping, Microneedle-assisted genome editing: A transdermal strategy of targeting *NLRP3* by CRISPR-Cas9 for synergistic therapy of inflammatory skin disorders. *Sci. Adv.* **7**, eabe2888 (2021).